$$g_1(x,y,z)=\tfrac{1}{3}(x^3+y^3)\tan^{-1}\frac{(x+y)^2-z}{\Gamma}+\tfrac{1}{2}\Gamma y\ln\{[(x+y)^2-z]^2+\Gamma^2\}+\tfrac{1}{3}[\Gamma\cdot\beta-\alpha(z+3y^2)]$$

$$\times\left\{\tan^{-1}\frac{x+y-\alpha}{\beta}+\tan^{-1}\frac{x+y+\alpha}{\beta}\right\}-\tfrac{1}{6}[\alpha\Gamma+\beta(z+3y^2)]\ln\frac{(x+y-\alpha)^2+\beta^2}{(x+y+\alpha)^2+\beta^2}-\tfrac{2}{3}\Gamma(x+y),$$

where

$$\alpha=\frac{1}{\sqrt{2}}[(z^2+\Gamma^2)^{1/2}+z]^{1/2},\quad \beta=\frac{1}{\sqrt{2}}[(z^2+\Gamma^2)^{1/2}-z]^{1/2}.$$

PHYSICAL REVIEW B VOLUME 1, NUMBER 4 15 FEBRUARY 1970

Shapes of Two-Phonon Recombination Peaks in Silicon†

N. O. FOLLAND
Kansas State University, Manhattan, Kansas 66502

(Received 14 April 1969; revised manuscript received 17 October 1969)

The radiative recombination spectrum of excitons in *n*-type Si exhibits structure which has been analyzed in terms of one- and two-phonon processes. A model for radiative recombination of excitons is presented which predicts one-phonon peak shapes which are in good agreement with experiment and two-phonon peak shapes which are in fair agreement with experiment. Calculations are described with particular attention devoted to phonon decoupling approximations. The observed width of the $\Delta_1(25)$ two-phonon peak is accounted for very well by phonon dispersion effects. Neither the $\Sigma_1(60)$ nor the $\Gamma_{25'}(64)$ two-phonon peak alone can span the observed width of the assigned peak. We conclude that this peak is composite. The calculations provide the following best estimates of the magnitudes (meV) of intervalley electron-phonon matrix elements $\Delta_1(25)$-261, $\Sigma_1(48)$-80, $\Sigma_1(60)$-178, and the intravalley (valence band) matrix element $\Gamma_{25'}(64)$-403 where the phonons are designated by their symmetry and energy (meV). Also included are certain intermediate results which show the effects of the approximations and permit modifications of the model to be tested without extensive calculation.

1. INTRODUCTION

STRUCTURE observed in the intrinsic radiative recombination spectrum of excitons in *n*-type Si can be understood in terms of one- and two-phonon processes.[1] Reasonable assignments of the phonons involved can be made on the basis of the selection rules and the experimental phonon spectrum.[1,2] However, some ambiguities remain which cannot be resolved by such considerations alone.

In this paper is presented a model for the calculation of the shapes of radiative recombination peaks. It is the purpose of this paper to show that the largest two-phonon peak is composite and has major contributions involving a Σ_1 intervalley phonon and a $\Gamma_{25'}$ intravalley phonon. Detailed calculations are described of the shapes of the principal two-phonon recombination peaks from Si. The calculations are of theoretical interest in that they lead to the evaluation of the absolute magnitudes of those electron-phonon matrix elements which control transport processes.[3,4] In previous calculations of this type, only the integrated intensities were used to relate the experimental results to the electron-phonon coupling constants.[1,5] There was no basis to choose between equally tenable interpretations. Besides clarifying the interpretation of the two-phonon peaks the calculations reveal the effects of decoupling approximations.

The many-valley picture of the band structure of Si is briefly reviewed in Sec. 2 in the context of radiative recombination. The exciton radiative recombination intensity is expressed quantitatively in terms of matrix elements between one-electron Bloch states in Sec. 3. In Sec. 4, various levels of approximation and the results obtained are described and discussed. Calculated results are compared with experiment and empirical values obtained for the electron-phonon coupling constants in Sec. 5. Finally, in Sec. 6, the present results and conclusions are discussed in light of related work.

† Work supported in part by the Office of Naval Research under Themis Contract No. N00014-68-A-0504.

[1] W. P. Dumke, Phys. Rev. **118**, 938 (1960).

[2] P. J. Dean, J. R. Haynes, and W. F. Flood, Phys. Rev. **161**, 711 (1967).

[3] D. Long, Phys. Rev. **120**, 2024 (1960).

[4] J. E. Aubrey, W. Gubler, T. Henningsen, and S. H. Koenig, Phys. Rev. **130**, 1667 (1963).

[5] N. O. Folland, Phys. Letters **27A**, 708 (1968).

2. MANY-VALLEY MODEL FOR RECOMBINATION

We consider a many-valley model for Si based on the calculated band structure[6] and the experimental phonon dispersion curves.[7,8] In n-type Si, the conduction-band minima occur at six equivalent points along the lines Δ in the Brillouin zone. At low temperatures and at low electron concentrations most of the electrons are weakly coupled to holes in the valence band to form excitons. We assume that the excitons form a Boltzmann distribution in energy which is undisturbed by the radiative recombination processes.

In the experiments performed by Dean *et al.*[2] on n-type Si, electrons were excited from the valence band by intense radiation from a mercury arc. The intrinsic recombination radiation was observed for emitted photon energies near and just below the indirect exciton gap energy. The dominant contributions to the recombination radiation involve excitons which decay with aid of momentum conserving phonons. For weakly coupled electrons and holes, the selection rules[9] are the same as those for the analogous free-electron free-hole recombination.

The dominant one-phonon processes which are allowed by the selection rules[10] are shown schematically in Fig. 1. At low temperatures, only phonon emissions need be considered. In a typical one-phonon process the transition to the virtual conduction-band state Γ_{15} is accompanied by the emission of a momentum conserving phonon [symmetry Δ_5 (TO)] followed by emission of a photon (symmetry Γ_{15}) in the transition to the $\Gamma_{25'}$ ground state. Symbolically, $\Delta_1(\Delta_5)\sim\!\!\rightarrow \Gamma_{15}\rightarrow \Gamma_{25'}$.

We also consider two-phonon (third-order) processes. In the dominant two-phonon recombinations, a momentum-conserving phonon is emitted in the transition from the initial state to a virtual state in a neighboring valley as shown in Fig. 2. The process continues to the ground state as in the one-phonon processes. Only Δ_1 and Σ_1 intervalley phonons are allowed by the selection rules. It should be emphasized that the selection rules preclude intervalley phonons of symmetry Σ_4 and intravalley optical phonons of symmetry $\Gamma_{25'}$ as the initiators of a two-phonon process. Another significant two-phonon process which is allowed by the selection rules is a one-phonon process followed by the emission of a $\Gamma_{25'}$ intravalley phonon. Thus, emission of a $\Gamma_{25'}$ intravalley optical phonon is allowed to terminate a two-phonon process but is not allowed to initiate one.

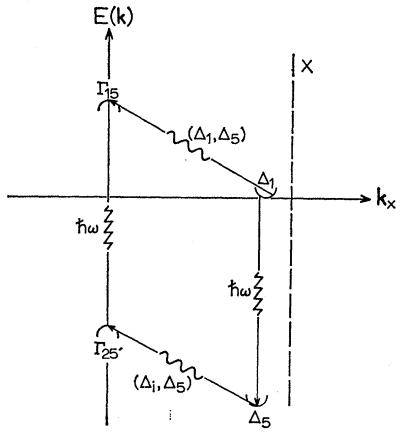

FIG. 1. One-phonon radiative recombination processes in Si. The symmetries of the allowed phonons are given in parentheses.

3. QUANTITATIVE FORMULATION

Using elementary time-dependent perturbation theory,[11] the recombination emission intensity (number of photons with angular frequencies within $d\omega$ of ω emitted from the material into a unit solid angle in unit time) from the radiative decay of an excitonic state A to the ground state of the electronic system F is

$$\tilde{I}_{A\to F}=\frac{2\pi}{\hbar}\sum_{B\cdots G}\left|\frac{H_{AB}(1)\cdots H_{GF}(N)}{(E_A-E_B-\Delta_1)\cdots(E_A-E_G-\Delta_{N-1})}\right|^2 \times\rho_E V\delta(E_A-E_F-\Delta_N), \quad (1)$$

where

$$\Delta_M=\sum_{j=1,M}\mathcal{E}_j,$$

and the $\mathcal{E}_j$ are photon or phonon energies and $\rho_E(\omega)=(n\hbar\omega)^2/(hc)^3$ is the photon density-of-states factor. Photon and phonon indices are suppressed as they are

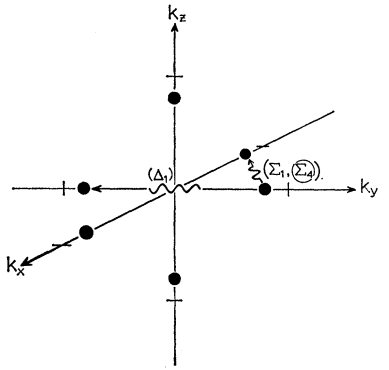

FIG. 2. Many-valley model for Si. Typical intervalley phonon processes are indicated by the wavy lines. The allowed phonon symmetries are given in parentheses. The Σ_4 intervalley phonon (circled) is forbidden by time reversal symmetry.

[6] G. Dresselhaus and M. S. Dresselhaus, Phys. Rev. **160**, 649 (1967).
[7] G. Dolling, *Inelastic Scattering of Neutrons in Solids and Liquids* (International Atimic Energy Agency, Vienna, 1965), p. 249.
[8] B. N. Brockhouse, Phys. Rev. Letters **2**, 256 (1959).
[9] N. O. Folland and Franco Bassani, J. Phys. Chem. Solids **29**, 281 (1968); M. Lax, Phys. Rev. **138A**, 793 (1965).
[10] Symmetry designations are in the notation of L. P. Bouckaert, R. Smoluchowski, and E. Wigner, Phys. Rev. **150**, 58 (1936).
[11] W. Heitler, *The Quantum Theory of Radiation* (Oxford University Press, New York, 1954), 3rd ed., p. 140.

implied by the electronic states. In all cases, we will assume that only one of the processes involves photon emission. The total emission intensity is obtained by taking an ensemble average in which each excitonic initial state is weighted by a Boltzmann factor according to its energy. We assume that thermal equilibrium is established despite recombination and that the exciton energy distribution is Maxwell-Boltzmann. The total intensity is

$$I_{A\to F}=\sum_A N_B(E_A)\tilde{I}_{A\to F}, \tag{2}$$

where N_B is the Boltzmann distribution function.

Following Dresselhaus's formulation[12] of the weak-coupling exciton problem the intensity may be expressed in terms of one-electron Bloch functions. The exciton geminal expanded in a product of Bloch states is

$$\phi^{\mathbf{K},n}(\mathbf{r}_e,\mathbf{r}_h)=\sum_{\mathbf{k},\mathbf{k}'}\delta_{\mathbf{K},\mathbf{K}'}F_n(\mathbf{q})\phi_{\mathbf{k}}(\mathbf{r}_e)\phi_{\mathbf{k}'}(\mathbf{r}_h), \tag{3}$$

where $\mathbf{K}'=\mathbf{k}+\mathbf{k}'$, $\mathbf{q}=\frac{1}{2}(\mathbf{k}-\mathbf{k}')$, and $F_n(\mathbf{q})$ is the Fourier transform of the exciton envelope function normalized so that $(V/2\pi)^3\int|F_n(\mathbf{q})|^2d^3q=1$. The Bloch-function momenta are written with respect to the conduction-band minima, $\mathbf{k}_e=\mathbf{k}_e{}^a+\mathbf{k}$ or the valence-band maximum, $\mathbf{k}_h=\mathbf{0}+\mathbf{k}'$. The Fourier transform of the exciton envelope function is a sharply peaked function of q. Neglecting the q dependence of the matrix elements and phonon energies, the intensity expression becomes

$$I_{A\to F}=\frac{2\pi}{\hbar}\sum_{a,b,\cdots d}N_B(E_a)\times\left|\frac{H_{ab}(1)\cdots H_{df}(N)}{(E_a-E_b-\Delta_1)\cdots(E_a-E_d-\Delta_{N-1})}\right|^2\times\rho(\omega)V\delta(E_a-\Delta_N). \tag{4}$$

The exciton energies E_b, ... are measured relative to the top of the valence band. The Boltzmann function is normalized, $(2\pi)^{-3}\int d^3K\,N_B(E_a(\mathbf{K}))=n_x$, where n_x is the exciton concentration. Equation (4) is our basic expression for the recombination emission intensity and represents the highest level of approximation that we consider. It is difficult to assess the approximations inherent in Eq. (4). But, we think that only the most subtle effects have been neglected and that it is meaningful to consider the effect of phonon decoupling approximations as they affect the results from Eq. (4).

Conservation of momentum requires that $\mathbf{k}_a=\mathbf{k}_p+\mathbf{k}_{a'}+\mathbf{G}$, where $\mathbf{G}$ is a reciprocal-lattice vector and $\mathbf{k}_p$ is the phonon momentum in the matrix element between Bloch states $\mathbf{k}_a$ and $\mathbf{k}_{a'}$. Since transition rates are largest when the energy denominators are smallest, it is energetically favorable for intervalley (intravalley) processes to precede (follow) transitions between electronic states which are well separated in energy. For example, the two-phonon process

$$\Delta_1(\Sigma_1)\rightsquigarrow\bar{\Delta}_1(\Delta_5)\rightsquigarrow\Gamma_{15}\to\Gamma_{25'}$$

is favored over a possible competing process

$$\Delta_1(\Delta_5)\rightsquigarrow\Gamma_{15}(\Gamma_{25'})\rightsquigarrow\Gamma_{15}\to\Gamma_{25'}$$

by a factor of 400 from the energy denominators alone. It is most improbable that variations in the matrix elements can compensate for this.

4. CALCULATIONS AND APPROXIMATIONS

Our objective is to evaluate Eq. (4) for the dominant radiative recombination processes. Since the energetically favored transitions involve virtual states very near the conduction-band minima, the conduction-band state Γ_{15} and the valence-band states Δ_5 and $\Gamma_{25'}$, the k dependence of the matrix elements can be neglected. This may be justified theoretically for the electronic states with $\mathbf{k}\cdot\mathbf{p}$ perturbation theory. We assume that the k dependence of the electron-phonon interaction may be neglected. Only phonon emission will be considered and the electron-phonon matrix elements are taken to be independent of temperature which is appropriate for low temperatures ($\lesssim 100°$K) and phonon energies $\mathcal{E}\gg k_BT$. It is convenient to define reduced matrix elements

$$H_{ab}(j)=\tilde{H}_{ab}(j)(k_BT)/\sqrt{N_0}, \tag{5}$$

where all energies are expressed in units of k_BT, $\tilde{\mathcal{E}}_j=\mathcal{E}_j\times k_BT$, $E_a=\tilde{E}_ak_BT$. The factors $\sqrt{N_0}$, where N_0 is the number of unit cells in the crystal, which occur in the usual expressions for the electron-phonon and photon emission matrix elements are included explicitly.

It is found, experimentally, that constant energy surfaces relative to the conduction-band minima are ellipsoids of revolution about the lines Δ

$$E(\mathbf{k})=E_0(a_{\parallel}k_{\parallel}{}^2+a_{\perp}\mathbf{k}_{\perp}{}^2), \tag{6}$$

where, if length is measured in Bohr radii, then $E_0=1$ Ry$=13.6$ eV and $a_{\parallel}\sim 1$ and $a_{\perp}\sim 5$. Except for the exciton energy shift we take the same K dependence for the exciton energy band as for the conduction band. Since the photon momentum is essentially zero, one sum over virtual states is omitted. This enters the intensity expression below as a δ function.

If the sums over electronic states are converted to integrals and the definitions and approximations described above are introduced, Eq. (4) becomes

$$I_{A\to F}=\frac{2\pi}{\hbar}(k_BT)|\tilde{H}_{ab}(1)\cdots\tilde{H}_{df}(N)|^2\times n_x\rho(\omega)\frac{\Omega_0{}^2}{(\pi)^{1/2}}\tilde{I}_N, \tag{7}$$

[12] G. Dresselhaus, J. Phys. Chem. Solids 1, 14 (1956); R. J. Elliott, Phys. Rev. 108, 1384 (1957).

where

$$\tilde{I}_N=2\left(\frac{2\Omega_0}{(2\pi)^3}\right)^{N-2}\frac{(k_BT)}{(2\pi)^3}\int d^3k_a\cdots\int \times\frac{N_B(\tilde{E}_a)\delta(E_a-\Delta_N)\delta(\mathbf{k}_i-k_{i-1})}{(\tilde{E}_a-\tilde{E}_b-\Delta_1)^2\cdots(\tilde{E}_a-\tilde{E}_d-\tilde{\Delta}_{N-1})^2} \quad (8)$$

is a dimensionless shape function.

Calculation of the one-phonon transition rates is trivial if the weak k dependence of the phonon energies involved is neglected. A typical one-phonon, $\Delta_1(\Delta_5)\sim\!\!\rightarrow \Gamma_{15}\rightarrow\Gamma_{25'}$ transition rate is given by

$$\tilde{I}_2=\frac{2(\sqrt{\tilde{E}})\exp(-\tilde{E})\theta(\tilde{E})}{(\tilde{E}-\tilde{E}_{\Gamma_{15}}-\mathcal{E}_{\Delta_5})^2}, \quad (9)$$

where

$$\tilde{E}=\mathcal{E}_{\downarrow}-(\tilde{E}_g-\mathcal{E}_{\Delta_5}),\quad \theta(x)=0(1),\quad \text{if}\quad x<(>)0.$$

The exciton gap energy is $E_g=1.155$ eV and $\mathcal{E}_{\downarrow}$ is the photon energy. It follows from Eq. (9) that the one-phonon transitions will exhibit a sharp threshold in photon emission at an energy $\mathcal{E}_{\Delta_5}$ below the exciton gap energy and that the peak in photon emission is $\frac{1}{2}k_BT$ above threshold energy. The observed one-phonon peaks are noticeably broader than predicted by Eq. (9).[13] Inspection of the phonon dispersion curves indicates that the Δ_5 phonon-energy dispersion is greatest in directions perpendicular to the line Δ,

$$\mathcal{E}_{\Delta_5}(\mathbf{k})\cong\mathcal{E}_{\Delta_5}{}^0+\mathcal{E}^1(k_1/k_0)^2, \quad (10)$$

where if $k_0=2\pi/a$, then $\mathcal{E}_{\Delta_5}{}^0=58$ meV and $\mathcal{E}^1=-12.7$ meV are consistent with the observed broadening and the main features of the phonon-dispersion curves.

In general, calculation of the two-phonon and higher-order transition rates must be done numerically. An approximation is suggested by the fact that initial electron states are restricted to a very small region in k space near the minima. Thus, the k dependence of these states which appears in the phonon energies should be small and may be negligible. If the k dependence of the phonon energy is neglected, the first integral of Eq. (8) can be evaluated

$$\tilde{I}_N=2\left(\frac{\Omega_0}{4\pi^3}\right)^{N-2}\int d^3k_b\cdots\int d^3k_d \times\frac{\sqrt{(\tilde{E})}\exp(-\tilde{E})\theta(\tilde{E})\delta(\mathbf{k}_i-\mathbf{k}_{i-1})}{(\tilde{E}-\tilde{E}_b-\tilde{\Delta}_1)^2\cdots(\tilde{E}-\tilde{E}_d-\tilde{\Delta}_{N-1})^2}, \quad (11)$$

where $\tilde{E}=\tilde{\Delta}_N-\tilde{E}_g$. From Eq. (11), it is easy to see how the momentum dependence of the phonon energies can affect the peak shape. Particularly for photon energies near the threshold ($\tilde{E}\sim0$), the change of the phonon energy by just a few meV will be a large change in the numerator of the integrand. For the intermediate states considered here, similar changes of the phonon energies in the denominator will have negligible effect. For photon energies near threshold the variation of the phonon energy with momentum often serves to truncate the integral via the θ function. Thus, truncation errors are less important here. For photon energies beyond the peak maximum truncation error becomes more important. In the spirit of the model it was necessary to restrict the regions of integration to k vectors near the minima. We expect that truncation errors will underestimate the high-energy tails of the two-phonon peaks, but will have little effect on the peak height or width.

The two-phonon transitions involving a Δ_1 (LA) intervalley phonon should be most sensitive to the approximations leading to Eq. (11). Fortunately, this is also the most symmetric case and both Eqs. (8) and (11) can be evaluated with equal facility. The momentum dependence of the Δ_1 phonon energy is approximated by a conical surface centered at $\mathbf{k}=0$. For small deviations $\mathbf{k}'$ from the intervalley momentum $\mathbf{k}_0$ (defined as the momentum transfer between valley minima)

$$\mathcal{E}(\mathbf{k}_0+\mathbf{k}')=25.0\text{ meV}+25.0\text{ meV}(|\mathbf{k}_0+\mathbf{k}'|/k_0-1). \quad (12)$$

"Exact" (points) and approximate calculations (smooth curve) for the Δ_1 intervalley phonon peak are compared in Fig. 3. The peak shape is not appreciably different in the two calculations and the peak height for the "exact" calculation, Eq. (8), is about 6% smaller

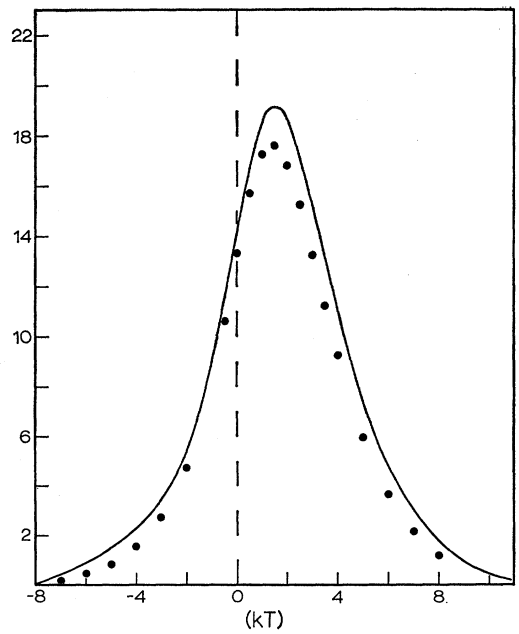

FIG. 3. The Δ_1 (25 MeV) two-phonon peak. The "approximate" calculations from Eq. (11) are given by the solid line and the "exact" calculations from Eq. (8) by the points.

[13] J. R. Haynes, M. Lax, and W. F. Flood, *Proceedings of the International Conference on Semiconductor Physics, Prague, 1960* (Academic Press Inc., New York, 1961), p. 423.

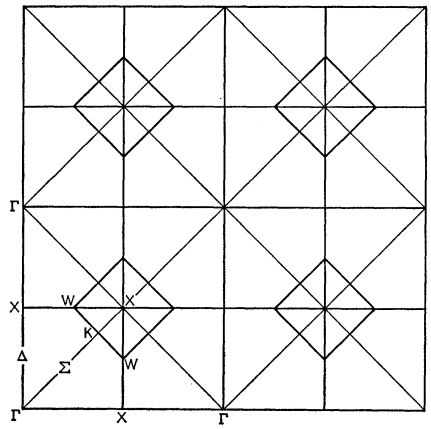

FIG. 4. The plane, $k_z=0$ in reciprocal space. Lines of special symmetry in or near the first Brillouin zone are marked in the notation of Bouckaert *et al.* The intervalley momentum vector $\mathbf{k}_\Sigma=(2\pi/a)$ (0.80, 0.80, 0) falls near the point K, but just outside the first Brillouin zone.

than the peak height found in the approximate calculation, Eq. (11). The two-phonon peak is about three times as wide at half-maximum as is the one-phonon peak, Eq. (9). If the phonon momentum dependence were neglected entirely, the two-phonon peaks would have the same shape as the one-phonon peaks.

We now consider the two-phonon peaks involving Σ_1 intervalley phonons with momenta near $\mathbf{k}^0=(2\pi/a)$ (0.80, 0.80, 0). The $k_z=0$ plane (Fig. 4) in reciprocal space shows the symmetry in perspective. It is difficult to measure high-energy phonon-dispersion curves as can be seen in Fig. 5 where the experimental points and estimated errors for the highest energy Σ_1 and Δ_5 phonon branches[7] are plotted together from the point $X[(2\pi/a)(1,1,0)]$. The momentum dependence of the phonon energies was approximated by a polynomial expansion about the point X consistent with the symmetry[14] and the experimental phonon data.

The Σ_1 two-phonon peaks calculated from Eq. (11) were narrower than the $\Delta_1(25)$ two-phonon peak by about a factor of 2. Even when a definite shoulder (shown by the broken line in Fig. 5) representing the extreme structure consistent with the $\Sigma_1(60)$ data was introduced the widths (2.4–$3.2k_BT$) were considerably less than the observed width ($4.2k_BT$). The lower $\Sigma_1(48)$ two-phonon peak as calculated from Eq. (11) also is only slightly broadened from the one-phonon peak shape. The $\Sigma_1(48)$ peak is observed in the shadow of the $\Sigma_1(60)$ peak and little can be said about its shape.

The remaining two-phonon process which is favored energetically and by the selection rules is completed by the emission of a $\Gamma_{25'}$ intravalley phonon. The phonon dispersion is approximated by

$$\mathcal{E}(\Gamma_{25'})=64.5\text{ meV}-7.0\text{ meV}(k'/k_0)^2, \qquad (13)$$

where $k_0=2\pi/a$ and k' is the momentum with respect to the point Γ ($k=0$). The shape of the $\Gamma_{25'}$ two-phonon peak is similar to the Σ_1 peaks, but because of the maximum in the phonon energy momentum relation, Eq. (13), the threshold is very sharp.

The main features of the peak shapes calculated from Eq. (11) are given in Table I. Although most of the table entries are self-explanatory, it should be emphasized that the entries labeled "calculated integrated intensity" should not be compared with the experimental integrated intensities. The calculated integrated intensities are defined as $\int \hat{I}_N(\tilde{E})d\tilde{E}$ with $\hat{I}_N$ given by Eq. (11). They may be used to calculate the electron-phonon coupling constants as described below or serve as the basis for other comparisons. For example, param-

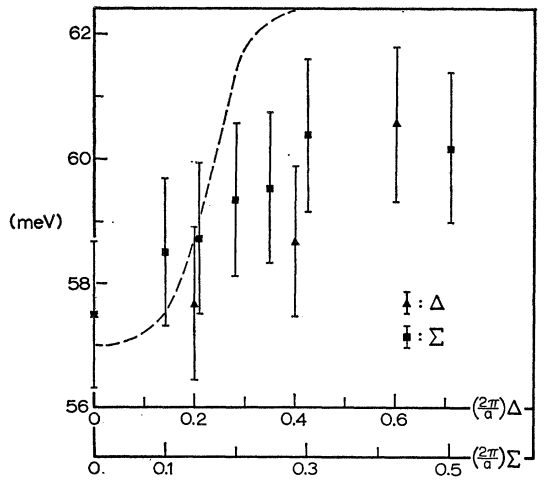

FIG. 5. Dolling's data and estimated errors (Ref. 7) are plotted relative to the point $\mathbf{k}_x=(2\pi/a)$ (1,1,0) on the same scale for the optical phonon branches Δ_5, $\mathbf{k}_\Delta=(2\pi/a)(0,0,x)$, and Σ_1, $\mathbf{k}_\Sigma=(2\pi/a)(x,x,0)$.

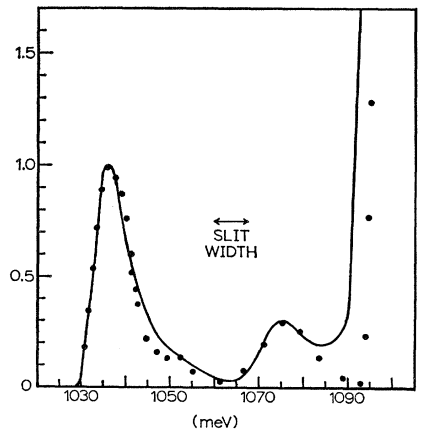

FIG. 6. Comparison of high-gain experimental radiative recombination two-phonon peaks (Ref. 2) (solid curve) with calculated peak shapes (points). A small constant background about 5% of the principal two-phonon peak was subtracted from the data.

[14] F. A. Johnson and R. Loudon, Proc. Roy. Soc. (London) **A281**, 274 (1964).

TABLE I. Calculated peak characteristics. All calculated quantities refer to Eq. (11). The one-phonon peak is labeled by its symmetry (Δ_5). The two-phonon peaks are labeled by the symmetry of the intervalley (intravalley) phonon. The threshold phonon energies listed correspond to the momentum for the prototype intervalley (intravalley) process. The peak maxima are displaced with respect to the threshold phonon energies as is exemplified in Fig. 3. The calculated integrated intensities [from Eq. (11)] should not be compared with the experimental integrated intensities (see text). At $T=26°\mathrm{K}$, $k_BT=2.24$ meV.

Peak type (symmetry)	one-phonon (Δ_5)	two-phonon (Δ_1)	two-phonon (Σ_1)	two-phonon (Σ_1)	two-phonon ($\Gamma_{25'}$)
Phonon energy (meV)	58	25	48	60	64.5
Displacement of max. from thres. (k_BT)	0.5	1.5	0.9	0.9	0.9
Width at $\frac{1}{2}$ max. (k_BT)	1.8	5.3	2.8	2.4	2.3
Height of max. (dimensionless)	2.4(−6)	1.9(−12)	2.3(−12)	2.2(−12)	2.8(−12)
Height of max. (decoupling approx.)	2.4(−6)	26.(−12)	19.(−12)	17.(−12)	16.2(−12)
Integrated intensity (calculated)	4.9(−6)	12.(−12)	7.2(−12)	5.8(−12)	6.1(−12)
Integrated intensity (decoupling approx.)	4.9(−6)	53.(−12)	39.(−12)	34.(−12)	33.(−12)
Integrated intensity (expl.)	1.0	0.032	0.010	0.030	0.040

eters obtained from the lowest level of approximation where phonon energy-momentum dependence is neglected entirely are given in Table I.

5. EMPIRICAL ELECTRON-PHONON MATRIX ELEMENTS

The procedure used to fit the experimental data was to superpose the calculated peaks as $\Sigma_i\hat{R}(i)\hat{I}(i)$, where for peak i, $\hat{R}(i)$ is the ratio of experimental to the calculated integrated intensity. Thus, fitting in this way to the experimental curve amounts to reestimating the experimental integrated intensities.

The Δ_1 two-phonon peak was chosen to determine the exact location of the conduction-band minimum because the calculated and experimental peaks both appear to be quite broad and the peak positions should not be influenced by finite slit-width effects. The conduction-band minimum found in this way lies at $\mathbf{k}=(2\pi/a)$ $(0.80\pm0.01, 0, 0)$ where most of the estimated uncertainty arises from the phonon-dispersion data. The Δ_1 peak does overlap with the $\Delta_5(58)$ one-phonon peak and the experimental integrated intensity is subject to interpretation. The Σ_1 phonon energies as determined by the 296°K data[7] are 48 and 60 meV (±1 meV), and the $\Gamma_{25'}$ phonon energy is 64 meV. The best fit to the recombination data was obtained when these energies were taken as 48, 60, and 64.5 meV as given in Table I.

The results of the curve fitting are shown in Fig. 6 where the experimental high-gain two-phonon radiative recombination spectrum[2] from which a small constant background contribution has been removed (5% of the principal two-phonon peak) is given by the solid line. The points represent the calculated emission intensity. Related experimental curves[2] indicate that the slits are of the order of 3–5 meV wide. The effect of finite slit widths was estimated by integrating the calculated intensity over a finite spectral region. The results are insensitive to the slit width.

As mentioned above the curve fitting procedure amounts to calculating the integrated intensity. Since the composite two-phonon peak is isolated it was chosen as the best estimate of integrated intensity relative to the one-phonon peak. A good fit (Fig. 6) was obtained when the integrated intensity for the Δ_1 two-phonon peak was doubled over the estimate given in Ref. 2.

The ratios of experimental to calculated integrated intensities are simply related to the electron-phonon matrix elements by Eqs. (7) and (8). The ratio of these quantities for the dominant one-phonon process and the observable two-phonon processes provide a good approximation to individual electron-phonon matrix elements,

$$N_i|\tilde{H}_{aa'}(i)|^2\cong\hat{R}(i)/\hat{R}(\Delta_5(58)), \qquad (14)$$

where $\hat{R}(i)$ is the ratio of experimental to calculated integrated intensities for the ith two-phonon process and $\hat{R}(\Delta_5(58))$ is the same ratio for the dominant one-phonon process. The number N_i takes specific account of the number of equivalent intervalley scattering options which might be initiated from a given valley, $N(\Sigma_1)=4$, $N(\Delta_1)=1$, and $N(\Gamma_{25'})=1$. The electron-phonon matrix elements calculated from Eq. (14) are listed in Table II, both for the detailed shape calculations and for the decoupling approximation.

TABLE II. Magnitudes of the electron-phonon matrix elements and related quantities. The matrix elements are labeled by the symmetry of the phonon involved. The intervalley scattering amplitude, Eq. (17), and the coupling constants, Eq. (16), are discussed in the text.

Phonon	Δ_1	Σ_1	Σ_1	$\Gamma_{25'}$
Phonon energy (meV)	25	48	60	65
Electron-phonon matrix element (meV)	261	80	179	403
Electron-phonon matrix element, decoupling approx. (meV)	54	18	33	77
Intervalley scattering amplitudes (relative)	0.70	0.14	0.55	...
Electron-phonon coupling constant [$(\mathrm{meV})^{-1/2}\ \mathrm{sec}^{-1}$]	1.12(+12)	0.43(+12)	2.1(+12)	2.7(+12)

The empirical electron-phonon matrix elements found above are the same ones that govern scattering by optical phonons in transport processes. The lifetime for scattering from a conduction (hole) state $\mathbf{k}_a=\mathbf{k}_a{}^0+\mathbf{k}'$ is given by

$$1/\tau(\epsilon_a(\mathbf{k}'))=g_{ia}(\epsilon_a(\mathbf{k}')-\mathcal{E}_{i0})^{1/2}\theta(\epsilon_a(\mathbf{k}')-\mathcal{E}_{i0}), \quad (15)$$

where the coupling constant g_{0a} is related to the electron-phonon matrix element by

$$g_{ia}=\left(\frac{\Omega_0}{a_0{}^3}\right)\frac{N_i|H_{aa'}(i)|^2}{\hbar\pi}\left(\frac{m_1{}^*m_2{}^*m_3{}^*}{(1\ \mathrm{Ry}m_0)^3}\right)^{1/2} \quad (16)$$

and $\mathcal{E}_{i0}$ is the energy of the optical phonon involved.

The coupling constants obtained from the empirical electron-phonon matrix elements are listed in Table II. The coupling constants defined above differ from the scattering amplitudes A_i defined by Long and used by him in his analysis[3] of the mobility of Si by a phonon energy and a proportionality constant,

$$A_i\propto g_{ia}/\mathcal{E}_{i0}. \quad (17)$$

The coupling constants and phonon assignments described above were used to repeat Long's analysis of the mobility of Si as a function of temperature. It was possible to reproduce Long's values of mobility as a function of temperature to within 8% between 100 and 300°K. It should be noted that the temperature dependence of the mobility is not very sensitive to the $\Sigma_1(60)$ coupling constant. As reported previously[5] the mobility curves were approximated equally well using a set of coupling constants based on an incomplete analysis of the recombination data. Our general conclusion here is that a fairly good fit can be obtained in the temperature range considered as long as the $\Sigma_1(60)$ coupling constant is not too small or zero. The fit obtained here would be improved if the ratio of the $\Sigma_1(60)$ to the $\Delta_1(25)$ coupling constant were increased.

6. DISCUSSION

The main conclusion resulting from our analysis of recombination radiation in Si is that the large two-phonon recombination peak is decomposed into peaks attributed to three independent processes. The largest contribution to this peak in terms of integrated intensity involves a $\Gamma_{25'}$ optical phonon and the remaining parts are from Σ_1 optical phonons. We are in substantial agreement with the original interpretation of radiative recombination in Si made by Dumke.[1] A discrepancy that has persisted between Dumke's analysis and the analysis of mobility data made independently by Long[12] is resolved.

One objection to our interpretation and conclusions is made by Onton[15] in the interpretation of his oscillatory photoconductivity data. He concludes that the $\Delta_1(25)$ and $\Sigma_1(48)$ phonons are evidenced as dips in the photoconductive response, but that no higher energy phonons may be seen, and therefore they are not involved. We note that this interpretation may be invalid because it is based on the original theory of Stocker and Kaplan[16] which does not apply in this context where more than one type of phonon is available for scattering. Calculations applicable to the case of Si which are based on an exact solution of the Stocker-Kaplan model for oscillatory photoconductivity are in progress.

The model described in this paper leads to one-phonon peak shapes which are in excellent accord with experiment and two-phonon peak shapes which are in fair agreement with experiment. Calculations which include the momentum dependence of the phonon energy fully account for the observed width of the Δ_1 two-phonon peak and require that all allowed two-phonon processes be operative to explain the principal two-phonon peak. In addition to the empirical electron-phonon matrix elements and coupling constants, we presented various intermediate results which display the effects of the approximations and permit simple modifications of the model to be tested without extensive calculation.

---

[15] A. Onton, Phys. Rev. Letters **22**, 288 (1969).
[16] H. J. Stocker and H. Kaplan, Phys. Rev. **150**, 619 (1966).